ACS OMEGA

http://pubs.acs.org/journal/acsodf

Article

Deactivation Mechanism and Regeneration of the CuCl/Activated Carbon Catalyst for Gas−Solid Acetylene Dimerization

Qi Song, Linye Liu, Qinqin Wang,* and Bin Dai*

Cite This: *ACS Omega* 2022, 7, 43265−43272

Read Online

ACCESS | Metrics & More | Article Recommendations | Supporting Information

ABSTRACT: Acetylene dimerization is necessary to the coal chemical industry for producing monovinylacetylene, while the deactivation mechanism and regeneration of catalysts have not been studied in detail, which is crucial to the design of high-efficiency catalysts for acetylene dimerization. Herein, the deactivation mechanism and regeneration methods of CuCl/activated carbon catalysts in gas−solid acetylene dimerization were studied in detail. The catalysts with different reaction times were analyzed by temperature-programmed desorption of ammonia (NH_3-TPD), Fourier transform infrared (FT-IR), thermogravimetry (TG), pyridine-FTIR, and X-ray photoelectron spectroscopy (XPS) analyses. NH_3-TPD results demonstrated that as the time went on, the strong acid in the samples was enhanced, while the weak acid was weakened. Similarly, pyridine-FTIR results indicated that both Brönsted and Lewis acids in the samples were decreased. TG and XPS results showed that the reasons for deactivation for acetylene dimerization in the gas−solid reaction were significantly affected by coke deposition and the change of Cu valence. The more the content of Cu^+, the higher the acetylene conversion rate, implying that Cu^+ may be the active center of the acetylene dimerization reaction. Thus, removing carbon deposition through calcining and increasing the content of Cu^+ was an effective way of regenerating the catalyst. This work strengthened the understanding of the deactivation behavior and provides a practicable regeneration method for the catalyst in gas−solid acetylene dimerization.

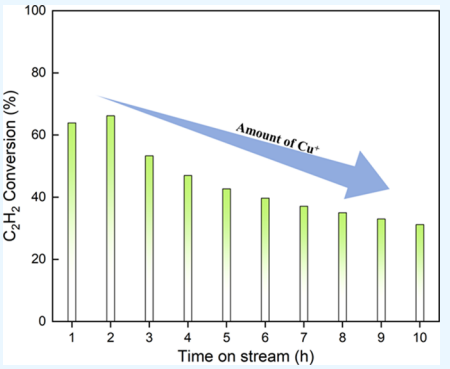

1. INTRODUCTION

The sources of acetylene will be cleaner, cheaper, and more extensive, which is along with the continuous development of a new technique for acetylene production by coal.[1] In addition, the price of petrochemical products remains high along with the increasingly exhausted crude oil resources and the rising price, creating a large profit space for downstream products of the acetylene chemical industry. Monovinylacetylene (MVA) as a downstream product of acetylene is an important fine chemical intermediate. It is prepared by the acetylene dimerization reaction and is widely used in the production of many important chemical products.[2] Consequently, acetylene dimerization is a significant reaction to produce MVA.

In the 1930s, the Nieuwland catalyst was invented and applied in industry. Owing to its convenient preparation, safety, and inexpensiveness, the catalyst still has been used until now. However, the catalyst has the disadvantages of low conversion and selectivity, many byproducts, and poor stability. Therefore, efforts were made to enhance the catalytic activity and stability of the catalyst. Han and co-workers reported that hydrochloric acid could restrain the production of precipitates, but too much hydrion had a negative effect on the reaction. It is beneficial for the life time of the catalyst and acetylene conversion, as the pH of the catalyst was controlled at 5.80−5.97 in the reaction process.[3] Meanwhile, decorating the catalyst with a ligand could strengthen the catalytic activity and selectivity.[4] Zhang et al. added various ligands to the Nieuwland catalyst in the aqueous-phase system. The research found the Nieuwland catalyst modified by the iminodiacetic acid, risedronic acid, and nitrogen-containing carboxylic acid, which could improve the reactivity and selectivity.[5−7] Compared with the aqueous-phase reaction system, the anhydrous catalyst had higher activity because the catalytic ions in the anhydrous catalyst had higher electron density.[8] Liu et al. studied the effects of different solvents on catalytic properties of acetylene dimerization. They pointed out that the yield of MVA was the highest as dimethylformamide was the solvent.[9] They also prolonged the lifetime of the catalyst by adjusting the acidity of the anhydrous catalytic system.[10] Furthermore, Liu et al. discussed that Cu^+ was transformed into Cu^{2+} which led to the deactivation of the catalyst. In addition, the Cu^{2+} could inhibit the transition from Cu^+ to Cu^{2+}, further enhancing the reactivity and catalyst life.[11]

Received: September 15, 2022
Accepted: November 4, 2022
Published: November 16, 2022

Compared with the gas−liquid reaction system, the gas−solid reaction system has the advantages of simple operation, easy separation and recovery of catalysts, high mass transfer rate, and so on. Li et al. used a CuCl/activated carbon (AC) catalyst in the gas−solid reaction system.[12] Subsequently, the $CuCl_2$ was added to the CuCl/AC catalyst for the reaction, and the acetylene conversion could reach 70.0%.[13] In recent years, researchers have made great progress in the gas−solid reaction system of acetylene dimerization, but the stability of the CuCl/AC catalyst is still not meeting the needs of real applications. Meanwhile, the deactivation mechanism of CuCl/AC in gas−solid acetylene dimerization is not yet known, so it is more than necessary that the catalysts are optimized for better utilization.

Based on this, in this study, catalysts with different reaction times were systematically discussed through many tests such as temperature-programmed desorption of ammonia (NH_3-TPD), Fourier transform infrared (FT-IR), thermogravimetry (TG), pyridine-FTIR, X-ray photoelectron spectroscopy (XPS), and so on. This work attempts to explain clearly the deactivation mechanism of CuCl/AC in gas−solid acetylene dimerization. In addition, a practicable regeneration method was also investigated in this work.

2. EXPERIMENTAL SECTION

2.1. Preparation of Catalysts. Catalysts were synthesized following a reported procedure.[13] Typically, 8.58 g of CuCl (97 wt %, Shanghai Macklin Biochemical Co., Ltd) and 3.83 g of ethanamine (98 wt %, Shanghai Macklin Biochemical Co., Ltd) were dissolved in the mixture (7 mL of DMF and 3 mL of 1, 4-dioxane, Shanghai Macklin Biochemical Co., Ltd) in a nitrogen atmosphere, which was stirred for 30 min at 80 °C. Then 5 g of coconut-shell AC (60−80 mesh, Tangshan United Carbon Technology Co., Ltd) was dispersed in the above solution, which was stirred for 120 min at 80 °C. The sample was further stirred for 10 h at 25 °C. Then the sample was filtered and dried under a vacuum oven for 12 h at 80 °C. Finally, the obtained sample was denoted as CuCl/AC.

In addition, samples were collected with different reaction times and named Sx (x = 0, 2, 4, 6, 8,10 h).

2.2. Acetylene Dimerization. Acetylene dimerization was carried out in a fixed bed microreactor made of stainless steel (40 cm in length, internal diameter 6 mm). The reaction temperature was set at 100 °C. The inflow of acetylene was set 4 mL/min. For the CuCl/AC catalysts (2 mL), the gaseous hourly space velocity was 120 h^{-1}. Before the heating, N_2 was flowed to the reactor for 30 min to get rid of air in the system. Then, acetylene was fed into the reactor as the temperature reached 100 °C. The gas chromatograph (Shimadzu, GC-2014C) was employed to confirm the composition of the products after washing.

2.3. Characterization. The morphology of the samples was analyzed by transmission electron microscopy (TEM, Tecnai G2 F20 S-TWIN 200KV). The crystal structure of the samples was determined by X-ray diffraction (XRD, Bruker D8 Advance powder diffractometer). The surface chemical state of the samples was characterized by X-ray photoelectron spectra (XPS, Thermo Scientific Escalab 250Xi). The coke content of the samples was investigated by a thermal gravimetric analyzer (TG, NETZSCH STA 449 F5/F3 Jupiter thermos gravimetric analysis). To obtain the TG profiles, the samples were heated from 50 to 800 °C (10 °C/min) in an air flow. The surface acidity was analyzed by NH_3-TPD (Auto Chemll 2920). The molecular structure of the samples was characterized using a Raman spectrometer (Raman, Renishaw inVia, measurement range: 100−3500 cm^{-1}, laser wavelength: 532 nm). The surface chemical structures of the samples were analyzed by Fourier transform infrared reflection (FTIR, Nicolet IS10). The elemental composition of the samples was analyzed by inductively coupled plasma optical emission spectroscopy (ICP-OES, Agilent ICPOES 730). Surface acidity of the samples was analyzed by FTIR-adsorbed pyridine (Py-FTIR, Thermo Nicolet 380).

3. RESULTS AND DISCUSSION

The catalytic performance of the CuCl/AC catalyst was tested in the acetylene dimerization reaction, as shown in Figure 1.

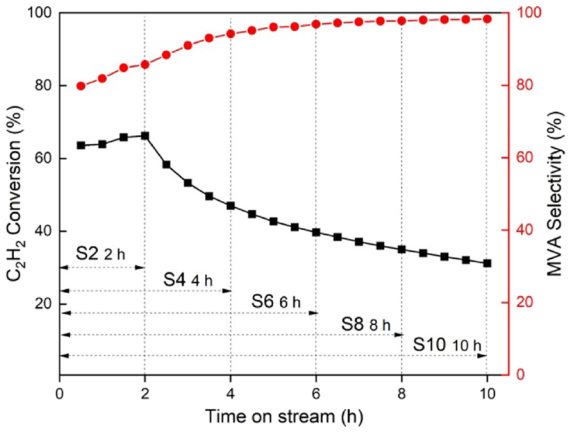

Figure 1. Catalytic activity of CuCl/AC in acetylene dimerization. Reaction conditions: 100 °C and space velocity 120 h^{-1}.

The conversion to acetylene was lightly raised at the initial reaction. Less obvious inactivation was observed over a period of 2 h. However, the reaction activity declined sharply after 2 h. When the reaction lasted for 6 h, it decreased by 20% compared with the initial stage. After that, the conversion of acetylene declined slowly, and the conversion to acetylene was 30% with 10 h time on stream. The conversion of total acetylene decreased by 36%. Moreover, at the early reaction stage, the selectivity of MVA was lightly raised and then came to a stable state. For the heterogeneous catalysis, the reasons for the supported catalyst inactivation were the loss of active sites, sintering of catalysts, or structures of catalyst change owing to instability or being covered/poisoned.[14] To dig the reasons for catalyst inactivation out, we performed the following tests on the samples.

The surface chemical structures of these samples were determined by FTIR (Figure 2). The signals of vibration at ∼3400 cm^{-1} were assigned to −OH.[15,16] As time went on, the signal strength of these peaks progressively decreased, indicating that the acidity of the samples changed during the reaction.[17] In the meantime, the signals of vibration at ∼1640 cm^{-1} in all samples were attached to −NH from ethanamine. Additionally, the signals of vibration at ∼1050 cm^{-1} were attributed to −C−O.[15] Furthermore, The signals of vibration at ∼1570 and 600 cm^{-1} were related to C═C and −C−H, respectively.[15]

The surface acidity of these samples was investigated by NH_3-TPD because the strength and distribution of acidity of the samples also had a major part to play in the reaction. NH_3-TPD profiles and NH_3 uptakes of these samples are presented

https://doi.org/10.1021/acsomega.2c05974
ACS Omega 2022, 7, 43265−43272

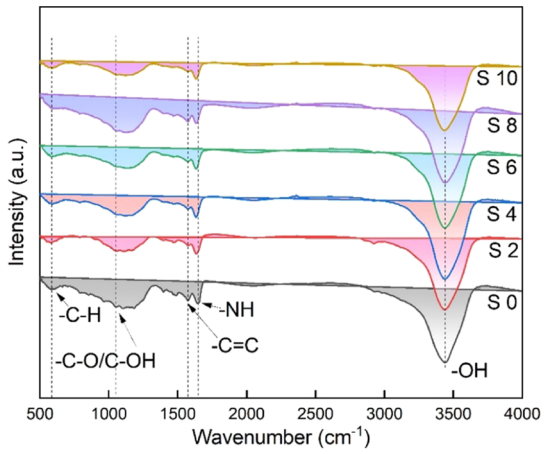

Figure 2. FTIR spectroscopy of the samples.

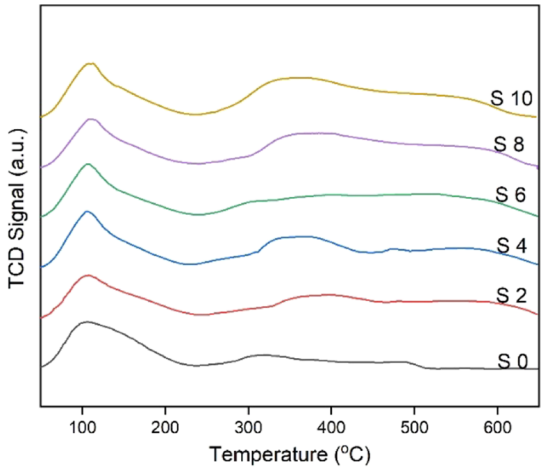

Figure 3. NH_3−TPD profiles of the samples.

in Figures 3 and S2 and Table 1, respectively. The peaks at ∼110 °C may be related to NH_3 desorbed from support channels. The peaks at 150−300 °C were assigned to weak acid sites. The peaks at 300−500 °C were related to strong acid sites.[18] The copper species could interact with ammonia molecules by forming Cu^x-NH_3 bonds.[19] In addition, the desorption peaks shown at ∼600 °C may also be assigned to the decomposition of the complex between copper and NH_3 of the samples.[20] Compared with an AC support, the adsorption quantity of ammonia was greatly increased in other samples. This was because a large amount of ammonia was adsorbed by the copper species in the samples, especially Cu^{2+} species.[19,20] As the reaction went on, the strong acid in the samples was improved as the Cu^{2+} increased. At the same time, CuCl could enhance the Brönsted acid in the samples, so that more ammonia was adsorbed on the samples.[20,21] In addition, with the increase of reaction time, the desorption peaks corresponding to strong acid sites lightly moved to higher temperature, suggesting that the acidity was a little enhanced. It was clear that strong acid was increased with the extension of the reaction time, which was unfavorable for catalyst stability because strong acid sites could accelerate the formation of coke.[22] It was quite evident that carbon deposition also increased with the increase of strong acid of the samples, as shown in Figure 8.

Because Brönsted and Lewis acid cannot be distinguished by NH_3-TPD, the pyridine adsorption IR spectra were employed to analyze the samples. Figure 4 shows the FT-IR spectra of

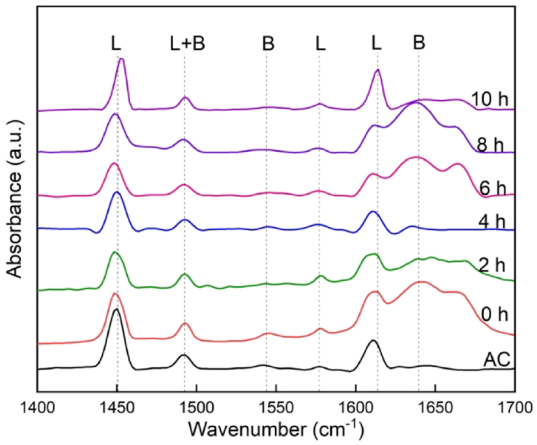

Figure 4. Pyridine-FTIR analysis of different samples measured at 100 °C.

pyridine desorption of these samples at the reaction temperature (100 °C). The signals at 1450 and 1540 cm^{-1} correspond to Lewis and Brönsted acids sites, respectively.[22,23] The relative amounts of two types of acids and their ratio (B/L) are listed in Table 2. Notably, by comparing the results from the described in NH_3-TPD analysis, two types of acid sites over these samples' surface displayed a much lower acidic amount (Figure 3). This was because of a great quantity of acid −OH over these samples' surface.[17,24] In NH_3-TPD profiles, the peaks at ∼300 °C were assigned to ammonia desorbed from Brönsted acid sites. The peaks at ∼350 °C were related to Lewis acid sites. It was notable that the dispersed copper species were Lewis type of acid sites.[18,19] In addition, it was

Table 1. Amount of Desorbed NH_3 of These Samples Tested by the NH_3-TPD

	ammonia amount (mmol/g)			
samples	weak acid (150 °C < T < 300 °C)	strong acid (300 °C < T < 500 °C)	total	W/S
AC	0.35	0.11	0.46	3.18
S0	1.05	3.45	4.50	0.30
S2	1.02	1.50	2.52	1.53
S4	0.89	1.83	2.72	0.48
S6	0.82	2.42	3.24	0.34
S8	0.73	2.61	3.34	0.28
S10	0.57	2.97	3.54	0.19

https://doi.org/10.1021/acsomega.2c05974
ACS Omega 2022, 7, 43265−43272

Table 2. Acidic Properties of These Samples Analyzed by Pyridine-FTIR

	acid amount (umol/g)			
samples	Brönsted	Lewis	Total	B/L
AC	2.81	24.38	27.19	0.11
S0	2.92	28.56	31.48	0.10
S2	2.50	23.76	26.26	0.11
S4	2.46	24.05	26.51	0.10
S6	1.62	24.83	26.45	0.07
S8	1.53	25.49	27.02	0.06
S10	1.45	25.84	27.29	0.06

known that Brönsted acid sites (Cu−OH) could be generated by the hydration of the bond between −OH and Cu.[18] However, the IR spectra indicated that the quantity of OH groups in the samples gradually reduced as the reaction was prolonged, resulting in the reduction of Brönsted acid in the sample. In addition, CuCl could enhance the acidity of Brönsted acid in the samples.[21] Therefore, the decrease of Brönsted acid in the samples may be related to the decrease of Cu^+. These may explain why Brönsted acid in the samples decreased. Extensive studies carried out showed that Lewis acid sites originated from the metal cations.[18] However, compared with Cu^{2+}, the acid strength of Cu^+ was weak.[25] According to the valence analysis of the copper element by XPS, Cu^+ in the surface of the fresh catalyst was oxidized to Cu^{2+}, resulting in the highest content of Lewis acid in the fresh catalyst. Compared with the fresh sample, a large amount of Cu^{2+} was reduced to Cu^+ or Cu^0 and carbon deposition in the samples was also becoming more and more serious with the reaction time increase, causing the metal sites on the surface to be covered.[22] For these reasons, the strength of Lewis acid in the samples decreased.

Figure 5a shows the Cu $2p_{3/2}$ XPS spectra of the samples. Two main peaks could be observed at binding energies of 932.9 and 934.8 eV which were associated with Cu^0/Cu^+ and Cu^{2+}, respectively. The satellite peaks at 941.8 and 944.5 eV correspond to Cu^0/Cu^+ and Cu^{2+}, respectively.[26,27] However, as previously reported, the binding energies of Cu^0 and Cu^+ (±0.1 eV) were too close to distinguish the valence states of Cu^0 and Cu^+ by Cu $2p_{3/2}$ analysis in XPS.[28] Thus, Cu LMM Auger patterns are shown in Figure 5b. The peaks at 915.7 eV were related to Cu^+ species, and the peaks at 911.0 and 918.4 eV were assigned to the Cu transition state and Cu^0 species, respectively.[29,30] In addition, proportions of Cu $2p_{3/2}$ species were quantitively given in Table 3. From Table 3, it is shown

Table 3. Proportion of Cu Species and Cu^+/Cu^{2+} Atomic Ratios of the Samples Based on XPS Characterization

	Cu $2p_{3/2}$ (%)			
samples	Cu^0	Cu^+	Cu^{2+}	Cu^+/Cu^{2+}
S0	0.8	6.2	93.0	0
S2	3.5	34.3	62.2	63.6
S4	2.9	25.1	72.0	47.0
S6	2.5	24.7	72.8	39.7
S8	3.9	23.1	73.0	35.0
S10	2.1	22.6	75.3	31.2

that the amount of Cu^{2+} was decreased and Cu^+ was increased at the initial reaction (during the first 2 h), which displayed the highest acetylene conversion. It might be speculated that the formation of the Cu active component during this process. Moreover, the Cu^0 and Cu^+ species increased with the reaction processing which could be attributed to the part of Cu^{2+} or Cu^+ was reduced to Cu^0 and Cu^+ by acetylene. However, as the reaction proceeded, it is clearly found that the amount of Cu^{2+} increased and Cu^+ decreased gradually, which may be because the Cu^+ was partially oxidized to Cu^{2+} and a part of Cu^+ was reduced to Cu^0 or covered by carbon deposition.[22] Moreover, the relationship between the conversion of acetylene and the amount of Cu^+ is clearly shown in Figure 6. The more content of Cu^+, the higher acetylene conversion rate, which further implied that Cu^+ may be the active center of the acetylene dimerization reaction.

It was well known that metal loss was another primary reason for catalyst inactivation. To evaluate the amount of metal loss in the samples, ICP-OES was performed in our experiments. From Table 4, the Cu component of all samples decreased slowly as the reaction progressed, which is one of the reasons for the deactivation.

Figure 7 shows the Raman spectra of these samples. The peaks were at around 1348 and 1582 cm^{-1}, which corresponded to the D and G bands of samples, respectively.[31] Generally, the D band was associated with the unordered sp^3

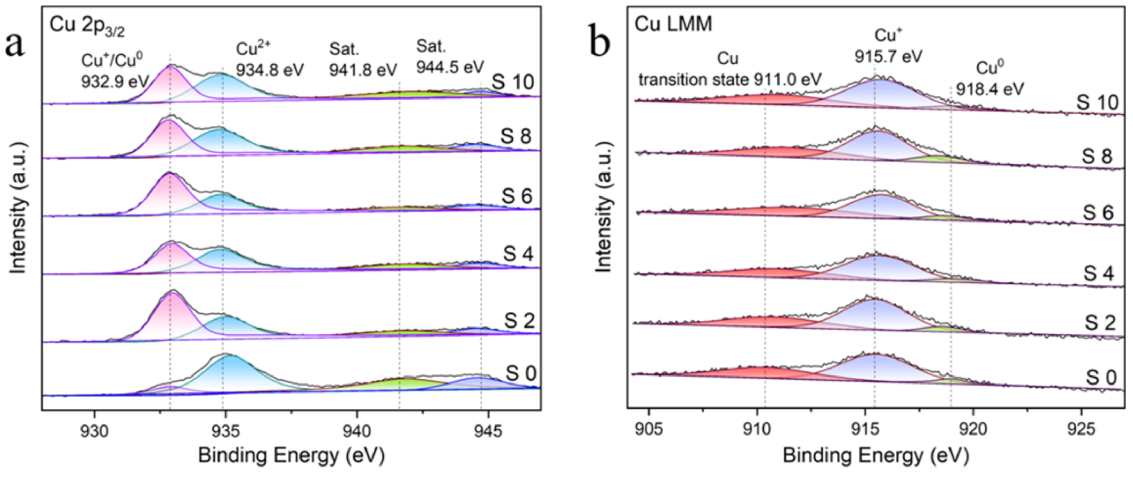

Figure 5. Cu $2p_{3/2}$ XPS spectra (a) and Cu LMM Auger spectra (b) of the samples.

https://doi.org/10.1021/acsomega.2c05974
ACS Omega 2022, 7, 43265−43272

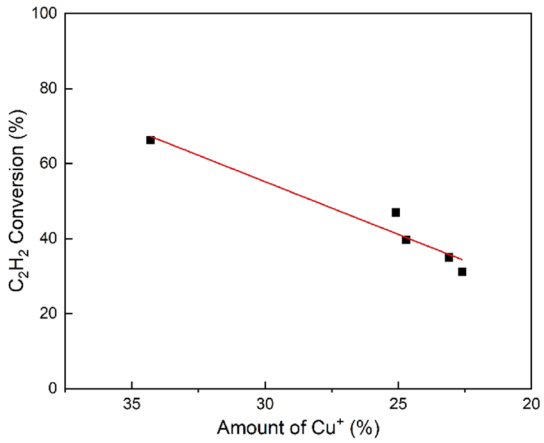

Figure 6. Relationship between the conversion of acetylene and the amount of Cu^+.

Table 4. Fraction of Cu in the Samples Derived from ICP-OES Analysis

	Cu elemental analysis	
samples	Cu wt %	the loss of ratios (%)
S0	21.44	
S2	21.16	1.31
S4	20.95	2.29
S6	20.90	2.52
S8	20.24	5.60
S10	20.23	5.64

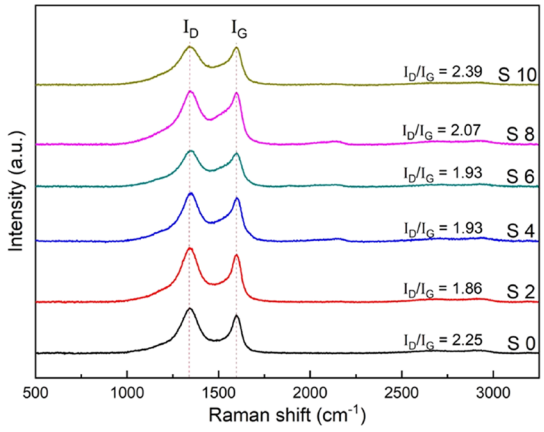

Figure 7. Raman analysis of different samples.

carbon and the G band was related to the sp^2 graphitic carbon. In addition, the area ratio of the two peaks (I_D/I_G) was most commonly used for evaluating the degree of graphitization and defects of the sample.[26] The Raman spectra showed an increasing trend of I_D/I_G value as time went on, which may be interpreted as the increase of carbon deposition or vacancies.[16] Meanwhile, the change of the I_D/I_G value suggests a larger unordered degree in the acetylene dimerization process.[15] This may be associated with the carbon deposition on the sample surface.

TG-DTA was employed to test the carbon deposition in the samples (Figure 8). The curves of similarity could be obtained at 110−200 °C in the samples. The slow downtrend may be associated with the desorption of the solvent. At 200−350 °C, the TG profiles of the used catalysts showed an obvious downtrend and the relevant DTA profiles exhibited sharp peaks. This may be related to the decomposition of hydrocarbon species or coke over the sample surface.[32] By calculation, the total amount of hydrocarbon or coke deposition of the used catalysts wase gradually increased with the increase of reaction time. Meanwhile, the TEM images in Figure S3 showed that coke was coated on the surface of the samples with the increasing time. According to analysis, coke deposition in the sample S10 was 7.8 wt %. As everyone knows, the metal sites were covered by coke deposition which may cause the deactivation of the catalyst.[22] It may cause the acetylene conversion to decrease by 36% from 66 to 30%. At 350−800 °C, the TG profiles decreased significantly, indicating the decomposition of AC.[13]

4. REGENERATION

It was certainly worth further exploring catalysts with high activity and stability, as well as developing an effective way of regenerating the catalyst. The regeneration of carbon-based catalysts by effectively eliminating deposits of carbon and keeping its structure were a challenging, as well as increasing the amounts of active sites of Cu^+. To verify this, 2 wt % CuCl was added to the sample S10, but the reactive of CuCl/AC was not recovered (Figure 10). This showed that only increasing the amount of Cu^+ was not enough. As shown in Figure S4, the TG profiles of the sample were regenerated in air (0.5 h, 250 °C). The loss of quality was dropped to the original state of the sample S0. From the result, coke deposition was successfully cleaned up. Although the deposit of coke could be removed, at the same time, the Cu^+ species were also reduced from the above catalyst. XPS demonstrated that a large number of Cu^+ on the catalyst surface was reduced or oxidized (Figure 9). As a result, the activity of CuCl/AC was still not recovered (Figure 10). Therefore, the regeneration of the catalyst required the combination of removing carbon deposition and increasing Cu^+ content.

As 2 wt % CuCl was added to the calcined catalyst, the reactivity was increased. In addition, the conversion of acetylene reached ∼69% as the addition amount of CuCl was 5 wt %, close to the fresh catalyst. This demonstrated that removing carbon deposition and increasing the content of Cu^+ was an effective way of regenerating the catalyst.

5. CONCLUSIONS

In summary, the catalysts with different reaction times were systematically analyzed with reaction activity and characterization experiments. The results revealed that with different reaction times, the strong acid was increased, while the weak acid was decreased. Similarly, both Brönsted and Lewis acids were decreased. In addition, this paper demonstrated that the reasons for deactivation for acetylene dimerization in the gas−solid reaction were significantly affected by coke deposition and the change of Cu valence. Carbon deposition could cover the active sites. Meanwhile, the more content of Cu^+, the higher acetylene conversion rate, implying that Cu^+ may be the active center of the reaction. Thus, the key points of improving the activity were exposing more active sites and reducing the carbon deposition. Regeneration by removing carbon deposition and adding Cu^+ appeared to be a viable option for recovering the reactivity, even though catalyst regeneration was still required to develop.

https://doi.org/10.1021/acsomega.2c05974
ACS Omega 2022, 7, 43265−43272

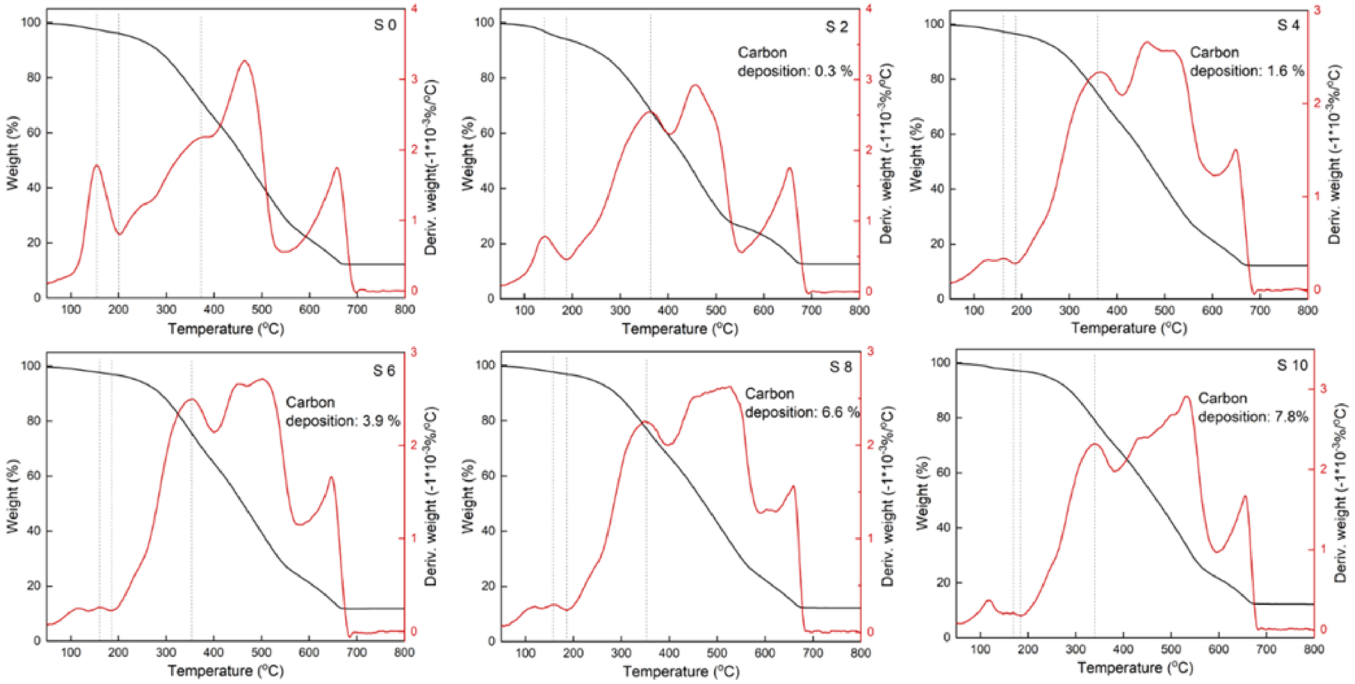

Figure 8. Thermogravimetry-differential thermal analysis (TG-DTA) curves of the samples.

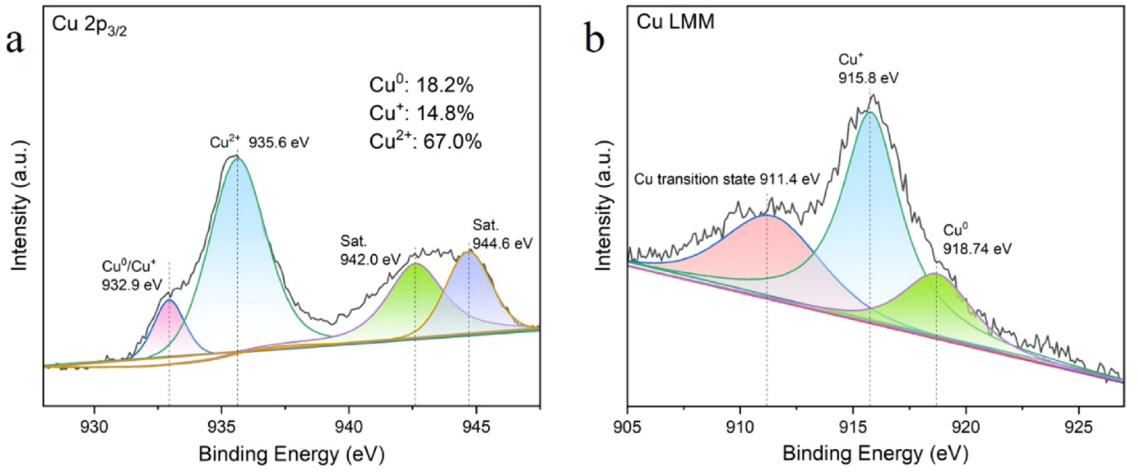

Figure 9. Cu 2p $_{3/2}$ XPS spectrum (a) and Cu LMM Auger spectra (b) of the catalyst after air treatment at 250 °C.

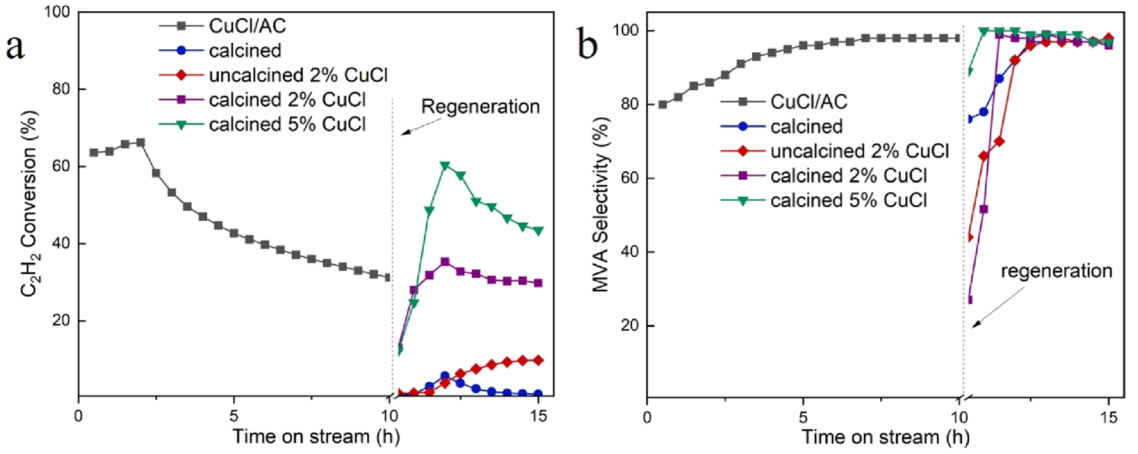

Figure 10. Catalytic activity of CuCl/AC and its catalytic activity upon regeneration by adding CuCl. (a)Conversion to acetylene and (b) selectivity of MVA. Reaction conditions: 100 °C and space velocity 120 h^{-1}.

https://doi.org/10.1021/acsomega.2c05974
ACS Omega 2022, 7, 43265−43272

■ ASSOCIATED CONTENT

Supporting Information

The Supporting Information is available free of charge at https://pubs.acs.org/doi/10.1021/acsomega.2c05974.

X-ray diffraction patterns; NH_3−TPD profiles; TEM images; and TG curves (PDF)

■ AUTHOR INFORMATION

Corresponding Authors

Qinqin Wang − *State Key Laboratory Incubation Base for Green Processing of Chemical Engineering, School of Chemistry and Chemical Engineering, Shihezi University, Xinjiang 832000, P. R. China;* orcid.org/0000-0002-9555-0712; Email: wqq_shzu@sina.com

Bin Dai − *State Key Laboratory Incubation Base for Green Processing of Chemical Engineering, School of Chemistry and Chemical Engineering, Shihezi University, Xinjiang 832000, P. R. China*; Email: db_tea@shzu.edu.cn

Authors

Qi Song − *State Key Laboratory Incubation Base for Green Processing of Chemical Engineering, School of Chemistry and Chemical Engineering, Shihezi University, Xinjiang 832000, P. R. China*

Linye Liu − *State Key Laboratory Incubation Base for Green Processing of Chemical Engineering, School of Chemistry and Chemical Engineering, Shihezi University, Xinjiang 832000, P. R. China*

Complete contact information is available at: https://pubs.acs.org/10.1021/acsomega.2c05974

Notes

The authors declare no competing financial interest.

■ ACKNOWLEDGMENTS

We gratefully acknowledge financial support provided by the High-level Talent Scientific Research Project of Shihezi University (No. RCZK201934 and No. SHYL-BQ201906) and the National Natural Science Funds of China (NSFC, 22178225).

■ REFERENCES

(1) Zheng, L.; Lin, R.; Luo, D.; Guo, L.; Zhang, J. Effect of Mg2+ additives on Nieuwland catalyst: The role of the second metal ionic radius. *J. Chin. Chem. Soc.* **2022**, *69*, 522−531.

(2) Zheng, L.; Lin, R.; Luo, D.; Guo, L.; Zhang, J. Dimerization of Acetylene to Monovinylacetylene (MVA) by Bimetallic Zr/Cu Catalyst in Nieuwland Catalytic System. *Molecules* **2022**, *27*, 602.

(3) Liu, J.; Zuo, Y.; Han, M.; Wang, Z.; Wang, D. Stability improvement of the Nieuwland catalyst in the dimerization of acetylene to monovinylacetylene. *J. Nat. Gas Chem.* **2012**, *21*, 495−500.

(4) Tachiyama, T.; Yoshida, M.; Aoyagi, T.; Fukuzumi, S. Mechanistic study on dimerization of acetylene with a Nieuwland catalyst. *Appl. Organomet. Chem.* **2008**, *22*, 205−210.

(5) Zhang, Q.; Li, C.; Luo, J.; Xie, J.; Zhang, J.; Dai, B. A novel risedronic acid-modified Nieuwland catalyst for acetylene dimerization. *Catal. Commun.* **2020**, *136*, No. 105922.

(6) You, Y.; Luo, J.; Xie, J.; Dai, B. Effect of Iminodiacetic Acid-Modified Nieuwland Catalyst on the Acetylene Dimerization Reaction. *Catalysts* **2017**, *7*, 394.

(7) You, Y.; Luo, J.; Xie, J.; Zhang, J.; Dai, B. Effects of Coordination Ability of Nitrogen-Containing Carboxylic Acid Ligands on Nieuwland Catalyst. *Catalysts* **2018**, *8*, 337.

(8) Liu, J. G.; Han, M. H.; Wang, Z. W. Studies on the Catalytic Performance of the Nieuwland Catalyst and Anhydrous Catalyst in the Dimerization of Acetylene to Monovinylacetylene. *Adv. Mater. Res.* **2012**, *550-553*, 312−316.

(9) Liu, J.; Han, M.; Wang, Z. Effect of solvent on catalytic performance of anhydrous catalyst in acetylene dimerization to monovinylacetylene. *J. Energy Chem.* **2013**, *22*, 599−604.

(10) Liu, J.; Zuo, Y.; Han, M.; Wang, Z. Improvement of anhydrous catalyst stability in acetylene dimerization by regulating acidity. *J. Chem. Technol. Biotechnol.* **2013**, *88*, 408−414.

(11) Liu, H.; Xie, J.; Liu, P.; Dai, B. Effect of Cu+/Cu2+ Ratio on the Catalytic Behavior of Anhydrous Nieuwland Catalyst during Dimerization of Acetylene. *Catalysts* **2016**, *6*, 120.

(12) Li, C.; Luo, J.; Zhang, Q.; Xie, J.; Zhang, J.; Dai, B. Gas−solid acetylene dimerization over copper-based catalysts. *New J. Chem.* **2019**, *43*, 13608−13615.

(13) Li, C.; Luo, J.; Zhang, Q.; Xie, J.; Zhang, J.; Dai, B. Cu(II)Cu(I)/AC Catalysts for Gas−Solid Acetylene Dimerization. *Ind. Eng. Chem. Res.* **2019**, *59*, 110−117.

(14) Li, X.; Li, P.; Pan, X.; Ma, H.; Bao, X. Deactivation mechanism and regeneration of carbon nanocomposite catalyst for acetylene hydrochlorination. *Appl. Catal. B: Environ.* **2017**, *210*, 116−120.

(15) Gan, G.; Fan, S.; Li, X.; Wang, L.; Yin, Z.; Wang, J.; Chen, G. Effects of oxygen functional groups on electrochemical performance of carbon materials for dechlorination of 1,2-dichloroethane to ethylene. *Chem. Eng. J.* **2022**, *434*, No. 134547.

(16) Kordek, K.; Jiang, L.; Fan, K.; Zhu, Z.; Xu, L.; Al-Mamun, M.; Dou, Y.; Chen, S.; Liu, P.; Yin, H.; Rutkowski, P.; Zhao, H. Two-Step Activated Carbon Cloth with Oxygen-Rich Functional Groups as a High-Performance Additive-Free Air Electrode for Flexible Zinc−Air Batteries. *Adv. Energy Mater.* **2018**, *9*, No. 1802936.

(17) Zhang, J.; Chen, J. Selective Transfer Hydrogenation of Biomass-Based Furfural and 5-Hydroxymethylfurfural over Hydrotalcite-Derived Copper Catalysts Using Methanol as a Hydrogen Donor. *ACS Sustainable Chem. Eng.* **2017**, *5*, 5982−5993.

(18) Wang, Y.; Li, H.; Wang, S.; Wang, X.; He, Z.; Hu, J. Investigation of sulphated CuCl2/TiO2 catalyst for simultaneous removal of Hg0 and NO in SCR process. *Fuel Process. Technol.* **2019**, *188*, 179−189.

(19) Jankowska, A.; Chłopek, A.; Kowalczyk, A.; Rutkowska, M.; Mozgawa, W.; Michalik, M.; Liu, S.; Chmielarz, L. Enhanced catalytic performance in low-temperature NH3-SCR process of spherical MCM-41 modified with Cu by template ion-exchange and ammonia treatment. *Micropor. Mesopor. Mater.* **2021**, *315*, No. 110920.

(20) Boosa, V.; Varimalla, S.; Dumpalapally, M.; Gutta, N.; Velisoju, V. K.; Nama, N.; Akula, V. Influence of Brønsted acid sites on chemoselective synthesis of pyrrolidones over H-ZSM-5 supported copper catalyst. *Appl. Catal. B: Environ.* **2021**, *292*, No. 120177.

(21) Wang, H.; Ma, S.; Zhou, Z.; Li, M.; Wang, H. Alkylation of isobutane with butene catalyzed by deep eutectic ionic liquids. *Fuel* **2020**, *269*, No. 117419.

(22) Lü, J.; Zhou, S.; Ma, K.; Meng, M.; Tian, Y. The effect of P modification on the acidity of HZSM-5 and P-HZSM-5/CuO-ZnO-Al2O3 mixed catalysts for hydrogen production by dimethyl ether steam reforming. *Chin. J. Catal.* **2015**, *36*, 1295−1303.

(23) Sebastian, J.; Zheng, M.; Li, X.; Pang, J.; Wang, C.; Zhang, T. Catalytic conversion of glucose to small polyols over a binary catalyst of vanadium modified beta zeolite and Ru/C. *J. Energy Chem.* **2019**, *34*, 88−95.

(24) Emeis, C. A. Determination of Integrated Molar Extinction Coefficients for Infrared Absorption Bands of Pyridine Adsorbed on Solid Acid Catalysts. *J. Catal.* **1993**, *141*, 347−354.

(25) Removal Mechanism of Thiophenic Compounds in Model Oil by Inorganic Lewis Acids. *Ind. Eng. Chem. Res.* **2012**, *51* (), 4682−4691, DOI: 10.1021/ie202831p.

(26) Xie, S.; Li, L.; Chen, Y.; Fan, J.; Li, Q.; Min, Y.; Xu, Q. Folic Acid Coordinated Cu-Co Site N-Doped Carbon Nanosheets for Oxygen Reduction Reaction. *ACS Appl. Mater. Interfaces* **2021**, *13*, 3949−3958.

(27) Huang, F.; Deng, Y.; Chen, Y.; Cai, X.; Peng, M.; Jia, Z.; Xie, J.; Xiao, D.; Wen, X.; Wang, N.; Jiang, Z.; Liu, H.; Ma, D. Anchoring Cu1 species over nanodiamond-graphene for semi-hydrogenation of acetylene. *Nat. Commun.* **2019**, *10*, 4431.
(28) Yang, L.; Pastor-Pérez, L.; Villora-Pico, J. J.; Sepúlveda-Escribano, A.; Tian, F.; Zhu, M.; Han, Y.-F.; Ramirez Reina, T. Highly Active and Selective Multicomponent Fe−Cu/CeO2−Al2O3 Catalysts for CO2 Upgrading via RWGS: Impact of Fe/Cu Ratio. *ACS Sustainable Chem. Eng.* **2021**, *9*, 12155−12166.
(29) Wang, B.; Jiang, Z.; Wang, T.; Tang, Q.; Yu, M.; Feng, T.; Tian, M.; Chang, R.; Yue, Y.; Pan, Z.; Zhao, J.; Li, X. Controllable Synthesis of Vacancy-Defect Cu Site and Its Catalysis for the Manufacture of Vinyl Chloride Monomer. *ACS Catal.* **2021**, *11*, 11016−11028.
(30) Arán-Ais, R. M.; Scholten, F.; Kunze, S.; Rizo, R.; Roldan Cuenya, B. The role of in situ generated morphological motifs and Cu(i) species in C2+ product selectivity during CO2 pulsed electroreduction. *Nat. Energy* **2020**, *5*, 317−325.
(31) Chen, X.; Fang, Y.; Lu, H.; Li, H.; Feng, X.; Chen, W.; Ai, X.; Yang, H.; Cao, Y. Microstructure-Dependent Charge/Discharge Behaviors of Hollow Carbon Spheres and its Implication for Sodium Storage Mechanism on Hard Carbon Anodes. *Small* **2021**, *17*, No. 2102248.
(32) Tian, S.; Wu, Y.; Ren, H.; Xie, H.; Zhao, Y.; Ma, Q.; Miao, Z.; Tan, Y. Insights into the deactivation mechanism of Zn-Cr binary catalyst for isobutanol synthesis via syngas. *Fuel Process. Technol.* **2019**, *193*, 53−62.

https://doi.org/10.1021/acsomega.2c05974
ACS Omega 2022, 7, 43265−43272